Shape control of thin deformable mirror with distributed piezoelectric sensors and actuators

Ahmed Tagui*, and *Mustapha* Sanbi

Advanced Sciences and Technologies Team, National School of Applied Sciences at Tetouan, Abdelmalek Essaadi University, Tetouan, Morocco

Abstract. This paper presents shape control of a thin piezoelectric deformable mirror in order to compensate the form errors caused by disturbances. The finite element model describing the dynamics of the mirror was obtained by Hamilton's principle and discretization was performed by nine nodes thin shell element according to the Kirchhoff-Love theory. The state space approach was used to generate matrices for control procedure. Because of the multivariable nature of the control problem involved in such structures and noise, the adaptive LQG-Kalman controller with multiple input-multiple output design was implemented to control the shape of the mirror. The proposed approach and related perspectives were finally discussed.

1 Introduction

Thin shell structures are widely used in civil engineering, aeronautics and space…etc. These structures could suffer from several mechanical actions of various forms. The deformations caused by the disturbances can generate dysfunctions. An example of such situation is encountered in a telescope which is based on the principle of two mirrors reflecting light to visualise distant objects in space. In fact the deformation of the mirrors in this case is a source of disorganization of the acquired image and degrades its quality.

The piezoelectric sensors and actuators were found to be quite effective in vibration (shape) control, thanks to their ability to transform mechanical deformations into electric load displacement and vice versa. However, most of the studies in literature have been dedicated to using these devices in structures having the form of plates or beams. There are relatively fewer works regarding deformation control of shell structures of general form by means of piezoelectric materials. Tzou and Gadre [1] proposed a multi-layered shell actuator theory for distributed vibration control of flexible shell structures. Tzou and Tseng introduced a new shell finite element formulation to model multi-layered shell sensor/actuator configuration [2]. Lee et al. [3] have extended the strain finite element formulation based on the nine-node shell to deal with actuator-embedded structures.

In this work, focus is on controlling the shape of a paraboloid mirror by means of two piezoelectric layers bonded on top and bottom of the shell faces. The structure is considered as a thin shell obeying the Kirchhoff-Love theory. The analysis of the behaviour is based on finite element discretization by nine-node shell elements. This allows formulating the state-space equations which are used then to define the law of control according to Linear Quadratic Gaussian (LQG) protocol associated with a Kalman filter.

2 Theoretical shell model

Let us consider an axisymmetric paraboloid shell with Z the axis of revolution and O the apex, see Fig. 1. The shell of thickness h has a mid-surface which can be parameterized by the meridian angle θ and the latitude angle ψ. This latter is the angle measured from the XY plane to the ray vector $\overrightarrow{OA}$.

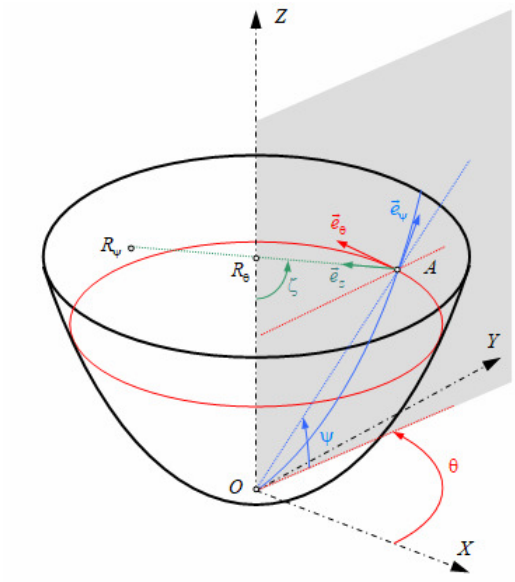

Fig. 1. Coordinates lines of the mid-surface of the paraboloid.

* Corresponding author: taguiahmed@gmail.com

Let $\vec{e}_\psi$ and $\vec{e}_\theta$ be the local unit vectors which are tangent in point A respectively to the coordinate lines ψ and θ. These two vectors are orthogonal because the coordinate ψ is taken on a meridian. So, they define the tangent plane to the mid-surface of the shell in point A. The inward normal to the mid-surface in point A is denoted $\vec{e}_z$. This normal forms angle ζ with the Z axis which is linked to ψ by: $\tan\zeta = 2\tan\psi$. ζ is also the angle that $\vec{e}_\psi$ forms with the horizontal in point A. The obtained local triad $(\vec{e}_\psi, \vec{e}_\theta, \vec{e}_z)$ is direct.

The position vector of a point A located on the mid-surface is given in the global triad $(\vec{e}_X, \vec{e}_Y, \vec{e}_Z)$ by

$$\vec{r}^{\,A} = R_0(\psi)\left(\cos\theta\vec{e}_X + \sin\theta\vec{e}_Y\right) + Z(\psi)\vec{e}_Z \tag{1}$$

where $Z(\psi)$ designates the position of a given parallel defined by latitude ψ and $R_0(\psi)$ is the radius of the parallel circle at that latitude.

Eq. (1) defines coordinates lines as parallel circles and meridian parabolas. The unit vectors of the local triad can be defined as

$$\begin{cases} \vec{e}_\psi = \dfrac{1}{\sqrt{R_0'^2 + Z'^2}}\left[R_0'\left(\cos\theta\vec{e}_X + \sin\theta\vec{e}_Y\right) + Z'\vec{e}_Z\right] \\ \vec{e}_\theta = -\sin\theta\vec{e}_X + \cos\theta\vec{e}_Y \\ \vec{e}_z = \dfrac{1}{\sqrt{R_0'^2 + Z'^2}}\left[-Z'\left(\cos\theta\vec{e}_X + \sin\theta\vec{e}_Y\right) + R_0'\vec{e}_Z\right] \end{cases} \tag{2}$$

where $R_0' = \partial R/\partial\psi$ and $Z' = \partial Z/\partial\psi$.

The position of a point M of the shell structure can be obtained by the following expression

$$\vec{r}^{\,M} = \vec{r}^{\,A} + z\vec{e}_z \tag{3}$$

The equation the parabolic trace on a meridian is assumed to be given by

$$Z = \frac{1}{4f}R_0^2 \tag{4}$$

where f is the distance separating the apex from the focal point.

Using Eq. (4), the parameterisation of the paraboloid in terms of the latitude angle writes

$$R_0(\psi) = 4f\tan\psi, \quad Z(\psi) = 4f\tan^2\psi \tag{5}$$

The chosen coordinates lines are directions of principal curvatures. The related radii of curvatures are given by

$$R_\psi = 2f\left(1+4\tan^2\psi\right)^{3/2}, \quad R_\theta = 2f\left(1+4\tan^2\psi\right)^{1/2} \tag{6}$$

In the following, the description of shell deformation is considered according to the Kirchhoff-Love theory. The displacement components (u, v, w) of a point of the shell are given in the triad $(\vec{e}_\psi, \vec{e}_\theta, \vec{e}_z)$ as [4]:

$$u(\psi,\theta,z) = \left(1+\frac{z}{R_\psi}\right)U_0(\theta,\psi) - \frac{z}{R_\psi}\frac{\partial W_0}{\partial\psi} \tag{7}$$

$$v(\psi,\theta,z) = \left(1+\frac{z}{R_\theta}\right)V_0(\theta,\psi) - \frac{z}{R_\theta\sin\psi}\frac{\partial W_0}{\partial\theta} \tag{8}$$

$$w(\psi,\theta,z) = W_0(\theta,\psi) \tag{9}$$

where U_0 and V_0 are the mid-surface displacements along the ψ and θ axes, respectively, and W_0 is the displacement in the normal direction z. Note that the displacements U_0, V_0 and W_0 are constant across the thickness of the shell.

The thin shell assumption can be used to simplify the relationship between displacement and strains. For a shell of revolution, one obtains the following expressions of dilatational strains [4]:

$$S_{\psi\psi} = \frac{1}{R_\psi}\left[\left(\frac{\partial V_0}{\partial\psi} + W_0\right) + z\frac{\partial\beta_\psi}{\partial\psi}\right] \tag{10}$$

$$S_{\theta\theta} = \frac{1}{R_\theta\sin\psi}\left[\frac{\partial U_0}{\partial\theta} + V_0\cos\psi + W_0\sin\psi + z\left(\frac{\partial\beta_\theta}{\partial\theta} + \beta_\psi\cos\psi\right)\right] \tag{11}$$

with the rotations given by

$$\beta_\psi = \frac{1}{R_\psi}\left(U_0 - \frac{\partial W_0}{\partial\psi}\right) \tag{12}$$

$$\beta_\theta = \frac{1}{R_\theta\sin\psi}\left(V_0\sin\psi - \frac{\partial W_0}{\partial\theta}\right) \tag{13}$$

3 Shape control

The paraboloid shell is assumed to be sandwiched between two piezoelectric layers consisting of distributed sensors and actuators bonded respectively on the inner face ($z>0$) and the outer face of the shell ($z<0$).

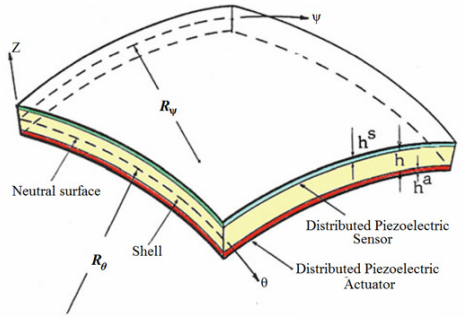

Fig. 2. Distributed piezoelectric sensor/actuator layers

Piezoelectric sensors/actuators can be lodged in discrete or continuous patches, see Fig. 2.

The desired form of the mirror is characterized by the Z coordinate of the mid-surface. Here, the problem is that for which the original form of the mirror is assumed to be known and the objective is to maintain this original form when the system undergoes deformation under some disturbance. Table 1 gives the displacement field in the three layers of the smart structure.

Table 1. The displacement field in each layer of the smart structure; Sensor $h/2 \le z \le h/2+h^S$, Mirror $-h/2 \le z \le h/2$, Actuator $-h/2-h^a \le z \le -h/2$

Layer	Displacement
Sensor	$u^S = \left(1+z/2R_\psi\right)U_0 - (z/2R_\psi)\partial W_0/\partial\psi$
	$v^S = \left(1+z/2R_\theta\right)V_0 - (z/2R_\theta \sin\psi)\partial W_0/\partial\theta$
	$w^S = W_0$
Mirror	$u^M = \left(1+z/R_\psi\right)U_0 - (z/R_\psi)\partial W_0/\partial\psi$
	$v^M = \left(1+z/R_\theta\right)V_0 - (z/R_\theta \sin\psi)\partial W_0/\partial\theta$
	$w^M = W_0$
Actuator	$u^a = \left(1+z/2R_\psi\right)U_0 - (z/2R_\psi)\partial W_0/\partial\psi$
	$v^a = \left(1+z/2R_\theta\right)V_0 - (z/2R_\theta \sin\psi)\partial W_0/\partial\theta$
	$w^a = W_0$

When the sensor layer deforms, the direct piezoelectric effect induces an electric potential. The induced charge can be collected from the sensor. Whereas, the converse piezoelectric effect is used by the actuator for controlling the shape of the shell.

It is assumed that the piezoelectric materials used are polarized along the z axis. Furthermore, the electric field $\vec{E}$ is taken to be irrotational (hypothesis of negligible magnetic effects) and can be expressed in terms of electrical potential φ as

$$\vec{E} = E_z\vec{e}_z = -\frac{\partial\varphi}{\partial z}\vec{e}_z \tag{14}$$

The linear electromechanical coupling constitutive equations for piezoelectric materials write

$$\vec{D} = e\vec{S} + \varepsilon^S\vec{E} \tag{15.1}$$

$$\vec{T} = c^E\vec{S} - e^T\vec{E} \tag{15.2}$$

where $\vec{T}$ is the stress vector, c^E is the elasticity matrix evaluated at constant electric field, $\vec{S}$ is the strain vector, e is the piezoelectric constant matrix, $\vec{E}$ is the electric field vector, $\vec{D}$ is the electric displacement vector, ε^S is the dielectric matrix evaluated at constant strain and $(\cdot)^T$ indicates the matrix transpose. Eq. (15.1) describes the direct effect and Eq. (15.2) the converse effect.

The transverse charge equation of piezoelectric sensor is given, for the case where $z \ll R_\psi$ and $z \ll R_\theta$, by [1,4]

$$\frac{\partial}{\partial z}\left[\left(e_{31}S_{\psi\psi} + e_{32}S_{\theta\theta} + \varepsilon_{33}E_z\right)R_\psi R_\theta \sin\psi\right] = 0 \tag{16}$$

where e_{31} and e_{32} are piezoelectric constants. For an isotropic transverse piezoelectric material $e_{32} = e_{31}$.

Eq. (16) can be used for sensor application. The expression of the potential at the output of the sensor having surface S^S is given in [4]. Because for a paraboloid shell: $\partial R_\psi/\partial\theta = 0$, the equation simplifies to

$$\begin{aligned}\varphi^S = \frac{h^S}{S^S}\int_S \Bigg\{ & h_{31}R_\theta \sin\psi\left[\frac{\partial U_0}{\partial\psi} + W_0 + r_\psi^S\frac{\partial}{\partial\psi}\left(\frac{U_0}{R_\psi} - \frac{1}{R_\psi}\frac{\partial W_0}{\partial\psi}\right)\right] \\ & + h_{32}\Bigg\{R_\psi\frac{\partial V_0}{\partial\theta} + U_0\frac{\partial(R_\theta\sin\psi)}{\partial\psi} + W_0R_\psi\sin\psi \\ & + r_\theta^S\Bigg[R_\psi\frac{\partial}{\partial\theta}\left(\frac{V_0}{R_\theta} - \frac{1}{R_\theta\sin\psi}\frac{\partial W_0}{\partial\theta}\right) \\ & + \frac{\partial(R_\theta\sin\psi)}{\partial\psi}\left(\frac{U_0}{R_\psi} - \frac{1}{R_\psi}\frac{\partial W_0}{\partial\psi}\right)\Bigg]\Bigg\}\Bigg\} d\theta d\psi\end{aligned} \tag{17}$$

where φ^S represents sensor local voltage amplitude, r_ψ^S and r_θ^S designate distances from the neutral surface to the mid-surface of the piezoelectric sensor, h_{31} and h_{32} are coefficients of the matrix related to open-circuit voltage at given strain. These coefficients can be calculated by $h = (\varepsilon^S)^{-1}e$. For an isotropic transverse piezoelectric material $h_{32} = h_{31}$.

To perform control, the actuator should apply a shape-shifting effort on the mirror structure in order to enable it to retrieve its original form. The voltage applied to actuators which is needed to generate such effort should be determined accordingly. The effective control force and moment induced by the imposed actuator potential φ^a can be expressed as [4]

$$N_{\psi\psi}^a = d_{31}Y^p\varphi^a \tag{18}$$

$$N_{\theta\theta}^a = d_{32}Y^p\varphi^a \tag{19}$$

$$M^a_{\psi\psi} = r^a_{\psi} d_{31} Y^p \varphi^a \tag{20}$$

$$M^a_{\theta\theta} = r^a_{\theta} d_{32} Y^p \varphi^a \tag{21}$$

where Y^p is Young's modulus of the piezoelectric actuator, r^a_{ψ}, r^a_{θ} are distance from the neutral surface to the mid-surface of the piezoelectric actuator, and d_{31}, d_{32} are piezoelectric strain constants. These constants can be calculated by $d = e(c^E)^{-1}$. For an isotropic transverse material: $d_{32} = d_{31}$.

The control forces and moments act as forcing terms in the electromechanical shell equations. These coincide with equations (2.4.10) to (2.4.14) given in [4].

4 FEM Formulation

In this analysis, the isoparametric finite element having nine nodes, [5], with four degrees of freedom per node $a_i = [U_{0i} \quad V_{0i} \quad W_{0i}]^T$ and φ_i is employed. Fig 3. shows the geometry of this curved shell element.

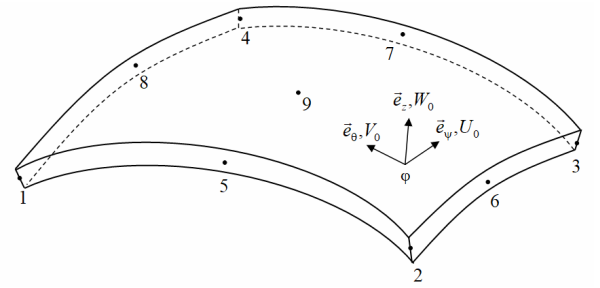

Fig. 3. Curved shell finite element having 9 nodes.

The displacement and potential are interpolated according to

$$a = [N_a] a^e \;, \quad \varphi = [N_\varphi] \varphi^e \tag{22}$$

where $[N_a]$ and $[N_\varphi]$ are the shape functions matrices as given in [5], a^e is the matrix of element unknown nodal displacements and φ^e is the matrix of element unknown nodal potentials.

The displacement and electric field matrices are determined by means of the following relations

$$S^e = [B_a] a^e \;, \quad E^e = [B_\varphi] \varphi^e \tag{23}$$

with $[B_a] = [\Delta][N_a]$ and $[B_\varphi] = -grad[N_\varphi]$, where $[\Delta]$ is the derivation operator [6] and $grad$ is the gradient operator.

Considering the action of body forces denoted P_b, pressure denoted P_s and concentrated load denoted P_c, along with a surface charge denoted q, the Hamilton's principle enables to derive the coupled electromechanical equilibrium equation. For any time instants t_0, t_1 and any given allowable arbitrary variation of displacement field and electric field, the associated formulation is given by following equation [4,7]

$$\begin{aligned} &\int_{t0}^{t1} \Big\{ \int_V \Big[\rho(\delta \dot{a})^T \dot{a} - (\delta S)^T \left[C^p \right]^T S + (\delta S)^T [e]^T E \\ &-(\delta E)^T [e]^T S - (\delta E)^T [\varepsilon]^T E + (\delta a)^T P_b \Big] dV \\ &+ \int_{\partial V} (\delta a)^T P_s dS_1 + \int_{\partial V} (\delta \varphi)^T q dS_2 + (\delta a)^T P_c \Big\} dt = 0 \end{aligned} \tag{24}$$

where ∂V is the surface area of the shell domain. The dot over a stands for time derivative.

Substituting the deformation and electrical field in the principle of variation, assembling after that the elemental quantities, one gets the global coupled electro-mechanical equations for shell structure with piezoelectric layers in a discrete matrix form as:

$$\begin{cases} [M]\ddot{a} + [K_{aa}] a + [K_{a\varphi}] \varphi = f \\ [K_{\varphi a}] a + [K_{\varphi\varphi}] \varphi = g \end{cases} \tag{25}$$

The matrices in the system of equations (25) are defined as:

$$[M] = \int \rho [N_a]^T [N_a] \, dV \tag{26}$$

$$[K_{aa}] = \int [B_a]^T \left[C^p \right] [B_a] \, dV \tag{27}$$

$$[K_{\varphi\varphi}] = \int [B_\varphi]^T [e] [B_\varphi] \, dV \tag{28}$$

$$[K_{u\varphi}] = \int [B_u]^T [e]^T [B_\varphi] \, dV = [K_{u\varphi}]^T \tag{29}$$

$$f = \int \rho [N_u]^T P_b \, dV + \int \rho [N_u]^T P_s \, dS \tag{30}$$

$$g = \int [N_\varphi]^T q \, dS \tag{31}$$

5 LQG-Kalman controller

To control the shape of the thin shell, the coupled electro-mechanical equations, Eq. (25), are converted into a space-state formulation [9]. The disturbances are pondered as white noise. The general equation of control can be written as

$$\dot{X} = [A] X + [B] U + W_1 \;; \quad Y = [C] X + W_2 \tag{32}$$

where X is the state vector, U the input control, Y the observation, $[A]$, $[B]$ and $[C]$ are the control matrices, W_1 and W_2 designate white Gaussian noise with mean equal to zero.

In the context of LQG control, the actuator inputs are fixed by minimizing the cost function J defined by

$$J = \lim_{\tau \to \infty} \frac{1}{\tau} \int \left\{ X^T [Q] X + U^T [R] U \right\} dt \tag{33}$$

where $[Q]$ and $[R]$ are respectively the state weighting matrix and control weighting matrix. These two matrices are obtained from the covariances of the two noise models which are assumed to be stationary over time as

$$Q = \overline{W_1 W_1^T}, \quad R = \overline{W_2 W_2^T} \tag{34}$$

where the bar designates the expectation.

In the closed-loop model, the potential φ^S output from the sensor as given by Eq. (17) is directly (or negatively) feed-back to the actuator φ^A [2]

$$\varphi^A = \mp[K]\varphi^S \tag{35}$$

where $[K]$ is the gain matrix.

The linear quadratic regulator (LQR), which is likely one of the most important results in optimal control, is applied next. The optimal value of the feed-back $[K]$ is then obtained as

$$[K] = R^{-1} B^T P \tag{36}$$

in which the unknown matrix P is determined from the following Riccati equation [8]

$$A^T P + PA - PBR^{-1}B^T P + Q = 0 \tag{37}$$

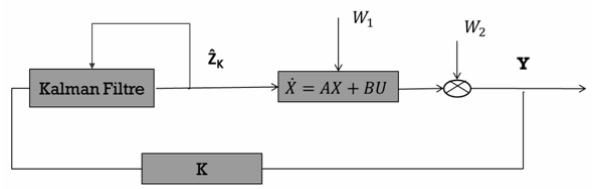

Fig. 4. Control system.

A Kalman filter is added for estimating the system state, based on prediction and current state measurement, see Fig. 4. This filter is defined by the following equation

$$\hat{Z}_k = \hat{Z}_{k-1} + [G_k]\left(Y_k - [C]\hat{Z}_{k-1}\right) \tag{38}$$

where $[G_k]$ is the Kalman gain matrix and $\hat{Z}_k$ the state estimate.

The first step of the Kalman filter is State Estimate {*prediction*} from the state-space model specified in Eq.(32). The next step is the Measurement Update {*Correction*} based on the residual (i.e. difference between the estimated and the measurement). The Kalman gain $[G_k]$ is computed at the second phase, so that the uncertainty in the state estimate is minimized.

The Kalman Gain is calculated as follows [10]

$$[G_k] = P_{k^-}[C]^T \left([C]P_{k^-}[C]^T + [R]\right)^{-1} \tag{39}$$

where P_{k^-} is the error covariance matrix of the current state, which could be considered as the uncertainty of this prediction. It is given by [10]

$$P_{k^-} = [A]P_{k-1}[A]^T + [Q] \tag{40}$$

The error covariance is updated by the next equation [10]

$$P_k = \left(I - [G_k][C]\right)P_{k^-} \tag{41}$$

6 Uncertainty quantification

Reliability of a numerical method used to solve partial differential equations of a model depends generally on several factors. These include the mathematical model, the numerical approximation (FEM), and the stochastic nature of disturbances. The errors related to the considered numerical method should be quantified and added to uncertainty that affects the model itself. The total error writes

$$Error = \varepsilon(\text{mod}) + \varepsilon(fem) + \varepsilon(pre) \tag{42}$$

The model error $\varepsilon(\text{mod})$ is associated to the chosen model (Kirchhoff-Love for "thin shells"; Reissner-Mindlin for "thick shells ",…).

When obtaining the space-state formulation via the FEM approach, a numerical error $\varepsilon(fem)$ resulting from discretization occurs. This error can be measured by the Richardson extrapolation method. While the solution converges asymptotically, the error $\varepsilon(fem)$ can be approximated as follows:

$$\varepsilon(fem) = \frac{R_1 - R_2}{r^p - 1} \tag{43}$$

where R_i is the obtained result with mesh h_i and $r = h_2/h_1 = h_3/h_4$ is mesh refinement ratio, and p is the order of convergence. This latter can be estimated by:

$$p = \frac{1}{\log(r)} \log\left(\frac{R_3 - R_2}{R_2 - R_1}\right) \tag{44}$$

As was presented in section 5, the Kalman filter is a model of prediction. Comparing model predictions and observations yields the prediction error $\varepsilon(pre)$. It is frequently assumed that the output measurement error is a normal stochastic variable with zero mean. The prediction error can be written as follows:

$$\varepsilon(pre) = s(pre) - s(true) \tag{45}$$

where $s(true)$ is the real state and $s(pre)$ is the predicted state.

7 Discussion

Using the Kirchhoff-Love shell theory and the FEM enables to get a modelling of general paraboloid mirror

for the purpose of shape control. The results can be obtained with the desired accuracy if the mesh is taken sufficiently small. In order to test the effectiveness of the control technique, a cantilevered three-layer paraboloid shell with two piezoelectric layers (actuator/sensor) bonded on the core shell was considered.

The material properties of the polyvinylidene fluoride PVDF are: Young's modulus $Y^p = 1.6GPa$, mass density $\rho^p = 1780kg/m^3$. The geometrical characteristics of PVDF patches are: thicknesses $h^a = h^s = 50\mu m$, the longitudinal arc length and the meridian arc length equal to $L_\psi = L_\theta = 100mm$, the focal distance equal to $50mm$. the dielectric permittivity is $\varepsilon_{33} = 8.85\times10^{-11} F/m$ and the piezoelectric constants are: $d_{31} = d_{32} = 6\times10^{-12} m/V$ and $e_{31} = e_{32} = 9.6\times10^{-3} C/m^2$, and. The Material properties of the core shell layer are: Young's modulus $Y = 90GPa$, Poisson's coefficients is $\nu = 0.3$ and mass density $\rho = 8700kg/m^3$. The shell thickness is $h = 1mm$.

The problem analytical solution was established using the double Fourier series as:

$$X(\psi,\theta) = \sum_i \sum_j X_{ij} \cos(\lambda_i \psi) \sin(\gamma_j \theta) \qquad (46)$$

with $\lambda_i = \pi i / L_\psi$ and $\gamma_j = \pi j / L_\theta$, and where X denotes U_0, V_0, W_0 or φ.

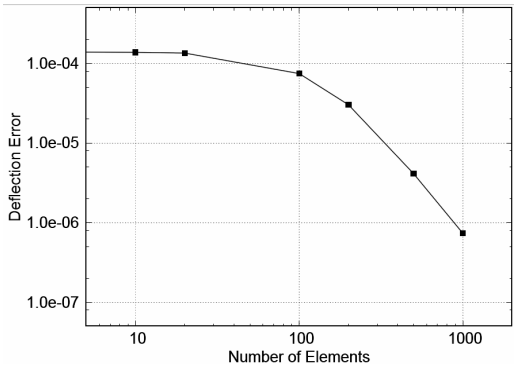

Fig. 5. Deflection error with the increasing number of elements in the simulation.

Considering comparison with the analytic solution, Fig. 5 presents the variation of numerical error $\varepsilon(fem)$ versus the number of elements used for shell meshing. It is seen that the error decreases monotonically as the number of elements is increased.

A state-space controller was proposed for the regulation of the paraboloid shape by means of distributed piezoelectric devices. This consists of a closed-loop including the LQG controller and the Kalman filter in order to manage noise effect on the dynamical state model. The measurement is performed based on the direct effect of the sensor piezoelectric layer, while the actuation is provided by the reverse effect and the controller feed-back.

The proposed approach of modelling and control was found to be quite effective in a previous work published by the authors [11] where the studied structure is a composite plate. So, the proposed modelling is expected to be successful for a paraboloid mirror. Note that further model reduction is to be performed in further work in order to enable real-time control of the paraboloid shell.

8 Conclusions

In this work, a straightforward approach to perform shape control of paraboloid mirrors by means of piezoelectric layers was developed. The kinematics of the layered shell was modelled according to the Kirchhoff-Love theory. An explicit parameterisation of the shell mid-surface by means of orthogonal coordinates lines was given. Then, the governing electromechanical equations were derived by using Hamilton's principle in terms of four degrees of freedom: three for the mid-surface displacements and one for the electric potential. The FEM formulation based on the nine nodes isoparametric curvilinear shell element with four degrees freedom per node was given.

Active shape control of a deformable mirror by means of distributed piezoelectric sensors and actuator was then proposed. The control law of actuation was elaborated through a closed-loop control approach consisting of the LQG controller and Kalman filtering.

The numerical FEM discretization error was quantified.

The actual model is useful in particular for assessing model reduction needed for real-time control of paraboloid mirrors in practical applications.

References

1. H.S. Tzou, M. Gadre, M, J. of Sound and Vibration **132**, 3 (1989)
2. H.S. Tzou, C. Tseng, J. of Sound and Vibration, 138,1 (1990)
3. S. Lee, N.S. Goo, H.C. Park, K.J. Yoon, C. Cho, Smart Mater. Struct. **12** (2003)
4. H.S. Tzou, *Piezoelectric Shells Sensing, Energy Harvesting, and Distributed Control-Second Edition* (Solid Mechanics and Its Applications, vol. 247, Springer Nature B.V., Dordrecht, 2019)
5. S. Ahmad, B.M. Irons, O.C. Zienkiewicz, Int. J. for Num. Meth. in Engineering **2**, 3 (1970)
6. S.C. Han, S. Choi, S.Y. Chang, Journal of Aerospace Engineering **19**, 2 (2006)
7. B. Koconis, P. Kollar, J. Compos. Mater. **28** (1994)
8. H. Kwakernaak, R. Sivan, *Linear Optimal Control Systems* (Wiley-Interscience, Hoboken, 1972)
9. L. Meirovitch, *Dynamics and control of structures* (John Wiley and Sons, Inc., New York, 1990)
10. B.D.O. Anderson, J. Moore, *Optimal Filtering* (Prentice-Hall Information and System Sciences Series, Englewood Cliffs, NJ, 1979)
11. L. El Khaldi, M. Sanbi, R. Saadani, M. Rahmoune, J. Compos. Sci. **242**, 7 (2022)